Thin liquid film flow over substrates with two topographical features

A. Mazloomi and A. Moosavi*

Center of Excellence in Energy Conversion (CEEC), School of Mechanical Engineering, Sharif University of Technology, Azadi Avenue, P. O. Box 11365-9567, Tehran, Iran

(Received 28 August 2012; published 26 February 2013)

A multicomponent lattice Boltzmann scheme is used to investigate the surface coating of substrates with two topographical features by a gravity-driven thin liquid film. The considered topographies are U- and V-shaped grooves and mounds. For the case of substrates with two grooves, our results indicate that for each of the grooves there is a critical width such that if the groove width is larger than the critical width, the groove can be coated successfully. The critical width of each groove depends on the capillary number, the contact angle, the geometry, and the depth of that groove. The second groove critical width depends on, in addition, the geometry and the depth of the first groove; for two grooves with the same geometries and depths, it is at least equal to that of the first groove. If the second groove width lies between the critical widths, the second groove still can be coated successfully on the condition that the distance between the grooves is considered larger than a critical distance. For considered contact angles and capillary numbers our results indicate that the critical distance is a convex function of the capillary number and the contact angle. Our study also reveals similar results for the case of substrates with a mound and a groove.

DOI: 10.1103/PhysRevE.87.022409 PACS number(s): 68.15.+e, 68.08.−p, 68.03.−g, 47.11.−j

I. INTRODUCTION

Understanding the behavior of thin liquid films flowing over topographical structures is essential in qualitative coatings of these substrates and has various applications, including in microelectronics [1–3], micro- and nanofluidics [4], displays and sensors [5], and heat-transfer processes [6,7]. Therefore, the subject has been extensively studied both experimentally [5,8–10] and theoretically [2,11–15].

In theoretical studies, the main approach is to use the lubrication approximation [11–13,15,16]. However, it is well known that the applicability of the lubrication theory is limited to small contact angles. Thus, other methods have been given attention. Gramlich *et al.* [2] studied the dynamics of thin liquid films over topographical structures by solving the Stokes equation via the biharmonic boundary integral method (BBIM). Alexeev *et al.* [10] studied Mrangoni convection and heat transfer in thin liquid films on heated walls with topography. In their study, the mobile gas-liquid interface was tracked by the volume-of-fluid method. Scholle *et al.* [17] studied the formation and presence of eddies within thick gravity-driven free-surface film flow over a corrugated substrate via the finite-element method. Sadigh *et al.* [18] studied falling thin liquid films on a substrate with complex topography using a three equation integral boundary layer system. Wang *et al*. [19] have studied the effects of height, the interval space and the cavitations depth on the electro-osmotic flow rate for both the homogenously and heterogeneously charged rough channels.

Recently, the lattice Boltzmann method (LBM) has been increasingly used to study various problems concerning fluids on structured substrates [20–30]. Dupuid and Yeomans [23,24] studied behavior of droplets on topographical substrates. They found that patterning can appreciably increase the contact angle. Huang *et al.* [26] investigated dynamics of droplets on grooved channels under a constant body force. It was found that for small scales the wettability and topography can considerably affect the drag on the droplet and the flow pattern. Hyväluoma *et al.* [27] performed simulations for slip flow on nanobubble-laden surfaces and showed that a strong shear can deform the bubbles and, thus, reduce the apparent roughness of the surface. Hyväluoma *et al.* [29] studied simulation of liquid penetration in paper and demonstrated that Shan-Chen multiphase model captures well the essential physics of capillary penetration. Chibbaro *et al.* [30] investigated the impact of wall corrugations in microchannels on the process of capillary filling and compared the results were compared against the Concus-Finn (CF) criterion for pinning of the liquid front at different contact angles.

The motivation for applying the LBM for the above problems stems from the fact that, in contrast to traditional numerical methods, which are based on discretizing the macroscopic equations of the continuum and momentum, the LBM is based on the microscopic models or mesoscopic kinetic equations. The LBM, because of the hyperbolic nature of the kinetic algorithms, can efficiently handle complex interfaces and geometries [31]. The characteristics are constant and the particles jump only from one lattice site to another one and this provides many advantages. Moreover, there is no need to consider any assumption for the relation between the contact angle and the contact line velocity because coalescence of the contact line is naturally treated by this method [32].

The LBM was developed originally from the lattice gas automaton (LGA) [33] and later was modified by modeling the LGA with a lattice Boltzmann equation. There are several LB schemes available for modeling multicomponent systems. The main methods include the recoloring process [34], the potential method [27,29,35–39], and the free-energy-based method [23,24,40].

In the recoloring model [34], Laplace's law is satisfied and formation of the interface between two fluids is done automatically. However, it is shown that in the perturbation step of the procedure, redistribution of the coloring functions

*moosavi@sharif.edu

creates anisotropic surface stress, which produces unphysical vortices near the interfaces [41]. Moreover, the main problems associated with the original LB color gradient method is the lattice pinning. Latva-Kakko and Rothman [42] have shown that this problem can be removed if the recoloring step is changed and wider interfaces are used. The method has been further extended by Halliday *et al.* [43] and Spencer *et al.* [44] to obtain a more efficient multicomponent LBM. Santos *et al.* [45] have proposed a field mediator's concept to the framework of the lattice-Boltzmann equation for simulating the flow of immiscible fluids which reduces computer processing. The method has been extended and applied for study via wetting in liquid-vapor systems [46] and capillary rise between parallel plates [47].

In the free-energy model the local momentum is conserved in addition to the overall momentum and this reduces the spurious velocity. However, the fundamental problem of this model is the effect of nonphysical effects of Galilean invariance [48]. There have been some efforts to remove this effect. It is shown that adding the density gradient to the pressure tensor can reduce this effect [40,49]. However, in this method, the problem is not removed completely. Also, for multiphase systems, it is shown that incorporating a correction term can considerably reduce the problem [50]. Li and Wagner [51] have proposed a method for multicomponent systems, which is based on the free energy, but in their method there has been no effort to remove the problem and the other, related, problem is that the viscosity and mobility are the same [51,52].

Systems with two immiscible liquids appear in various important applications. Relevant to our study, examples are two-layer slot coating [53], film formation during the spin-coating process [54], reverse roll coating flow [55], and double-layer coating in a wet-on-wet optical fiber coating process [56]. Among the models available for such multicomponent systems, the potential method has been used extensively for different applications because of its simplicity and flexibility [27,29,35–39]. The surface tension in this model is isotropic and conservation of the overall momentum is satisfied completely. One of the concerns in this method is the thermodynamic inconsistency [57]. However, Sbragaglia *et al.* [58] have shown that adding a gradient force, which has a fairly negligible effect on the evolution of the system, can make this model compliant with a free-energy functional. This may help to explain why this method is successful in various applications [37,59–64].

II. DESCRIPTION OF THE PROBLEM

Despite various studies conducted on the dynamics of thin liquid films on textured substrate and determining the required conditions for successful coating [1–3,10–13,15,17,18], to our knowledge, there is no research on the effect of a groove (or any other topographical texture) on the coating of the subsequent grooves in the flow direction. This is important, as generically the substrates contain many grooves and the required conditions for successful coating of these substrates may differ completely from those with a single groove.

In the present study, our main purpose is to examine the effects of various parameters such as the capillary number

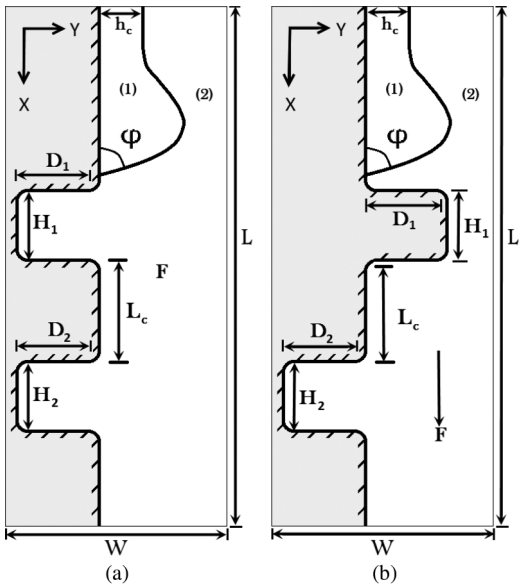

FIG. 1. A schematic representation of the contact line motion over textured substrate. A topographical substrate with two grooves (a) and a mound and a groove (b).

and the contact angle on the coating of a surface with two topographical features. As depicted in Fig. 1 we consider two immiscible and Newtonian fluids with viscosities μ_1 and μ_2 and densities ρ_1 and ρ_2. The surface tension between the fluids is equal to σ. An external force F, which is proportional to the gravity, is applied to the system and the liquid film under influence of this force is moving downward while the advancing front of the film flow is making a dynamic contact angle equal to ϕ with the substrate. In order to simulate the system, a rectangular region with the size $L \times W$ in the directions x and y, respectively, is considered (see Fig. 1). It is shown that for the upward positions, far from the contact line, the interface becomes parallel to the substrate with a thickness equal to h_c and the average velocity is given by $\bar{u}_c = \rho_1 g h_c^2/3\mu_1$, where g is the gravitational acceleration. Therefore, in order to avoid tangible changes in the average velocity or thickness of the film near the inlet ($x = 0$) and the outlet ($x = L$), the following boundary condition is applied:

$$\frac{\partial \mathbf{u}}{\partial x} = 0 \quad \text{at} \quad x = 0, L, \tag{1}$$

where $\mathbf{u} = (u, v)$ represents the velocity vector. On the solid surfaces it is assumed that the surfaces are impermeable,

$$\mathbf{u} = 0 \quad \text{on} \quad S, \tag{2}$$

where S represents the interface between the solid and the fluids. At the boundary $y = W$ a constant pressure P is considered:

$$P = \text{const} \qquad \text{at} \quad y = W. \tag{3}$$

All the corners that connect two plane surfaces have a dimensionless radius $r = 0.4$ and the dimensions are scaled with the film thickness in the inlet (h_c). In order to provide the basic information for the subsequent considerations, we, first, try to find the required conditions for successful coating of a surface with a U- or V-shaped groove. The case with a

U-shaped groove has been already studied using the boundary integral method with constant elements [2]. However, for considering such a method, the numerical slip was used to tackle the singularity at the contact point and it was assumed that the film at the contact position makes a contact angle equal to the equilibrium contact angle [65]. In order to check the results and validity of such assumptions, we consider this structure again and compare our results with those of Ref. [2].

The paper is organized as follows: the next section explains the numerical technique used in the study. The results and discussion are presented in Sec. IV. In the first parts of this section, calculation of the surface tension and verification of the numerical algorithm have been described. The results for different topographical features then are given. Finally, the last section summarizes the key findings of the study.

III. THE NUMERICAL METHOD

In order to study the problem, we use a multicomponent lattice Boltzmann method from Shan and Chen [35–37]. Considering the equivalence between the lattice Boltzmann algorithm and the incompressible form of the Navier-Stokes and the continuity equations, the Boltzmann equation can be discretized as follows [66]:

$$f_i^k(x+e_i\delta_t,t+\delta_t)-f_i^k(x,t)=\frac{f_i^k(x,t)-f_i^{k(\mathrm{eq})}(x,t)}{\tau_k}, \tag{4}$$

where the distribution function $f_i^k(x,t)$ is a scalar quantity which describes the probability of finding a fluid particle at location x in the direction i and the time t for the kth component. Therefore, it has a real and non-negative value. This quantity can specify all the macroscopic properties and also determine the dynamics of the system [67]. δ_t represents the time increment. On the right-hand side of the equation, τ_k is the relaxation time of the kth component in lattice units [67]. Also, $f_i^{k(\mathrm{eq})}(x,t)$, on the right-hand side, is the equilibrium distribution function and is derived from the following relation [63,68,69]:

$$\begin{aligned}
f_i^{k(\mathrm{eq})} &= \eta_k\rho_k-\frac{2}{3}\rho_k\mathbf{u}_k^{\mathrm{eq}}\cdot\mathbf{u}_k^{\mathrm{eq}} \qquad (\text{for} \quad i=0),\\
f_i^{k(\mathrm{eq})} &= \frac{(1-\eta_k)\rho_k}{5}+\frac{1}{3}\rho_k\left(\mathbf{e}_i\cdot\mathbf{u}_k^{\mathrm{eq}}\right)+\frac{1}{3}\rho_k\left(\mathbf{e}_i\cdot\mathbf{u}_k^{\mathrm{eq}}\right)^2\\
&\quad-\frac{1}{6}\rho_k\mathbf{u}_k^{\mathrm{eq}}\cdot\mathbf{u}_k^{\mathrm{eq}} \qquad (\text{for} \quad i=1,\ldots,4),\\
f_i^{k(\mathrm{eq})} &= \frac{(1-\eta_k)\rho_k}{20}+\frac{1}{12}\rho_k(\mathbf{e}_i\cdot\mathbf{u}_k^{\mathrm{eq}})+\frac{1}{8}\rho_k\left(\mathbf{e}_i\cdot\mathbf{u}_k^{\mathrm{eq}}\right)^2\\
&\quad-\frac{1}{24}\rho_k\mathbf{u}_k^{\mathrm{eq}}\cdot\mathbf{u}_k^{\mathrm{eq}} \qquad (\text{for} \quad i=5,\ldots,8),
\end{aligned} \tag{5}$$

where $\rho_k=\sum_i f_i^k$ represents the macroscopic density for the kth component and $\rho_k\mathbf{u}_k=\sum\mathbf{e}_i f_i^k$ with $\mathbf{u}_k$ as the macroscopic velocity of kth component. η_k is a free parameter that, via $(c_s^k)^2=\frac{3}{5}(1-\eta_k)$, is related to the sound speed in the region that includes component k [69]. In the study, we consider $\eta_k=4/9$ so $c_s^k=1/\sqrt{3}$ [63]. $\mathbf{e}_i$'s represent the discrete velocities and for a D_2Q_9 lattice are given by

$$\mathbf{e}_i=\begin{cases}0,0 & i=0\\ \cos\frac{(i-1)\pi}{2},\sin\frac{(i-1)\pi}{2} & i=1-4\\ \sqrt{2}\left(\cos\left[\frac{(i-5)\pi}{2}+\frac{\pi}{4}\right],\sin\left[\frac{(i-5)\pi}{2}+\frac{\pi}{4}\right]\right) & i=5-8.\end{cases} \tag{6}$$

The macroscopic velocities can be calculated from

$$\rho_k\mathbf{u}_k^{\mathrm{eq}}=\rho_k\mathbf{u}'+\tau_k\mathbf{F}_k, \tag{7}$$

where $\mathbf{u}'$ is a common velocity that is added to the equilibrium velocity of each part because of the interactions between the particles. $\mathbf{F}_k=\mathbf{F}_{1k}+\mathbf{F}_{2k}+\mathbf{F}_{3k}$ is the total force exerted on kth component and $\mathbf{F}_{1k}$, $\mathbf{F}_{2k}$, and $\mathbf{F}_{3k}$ are the forces due to fluid-fluid interactions, fluid-solid interactions, and the gravity, respectively [66]. Assuming that the equilibrium velocity is equal to the common velocity $\mathbf{u}'$ ($\mathbf{F}_k=0$) and because in this condition total momentum of all the particles should be preserved by the collision operator, using the multicomponent LBM we have

$$\mathbf{u}'=\left(\sum_k\frac{\rho_k\mathbf{u}_k}{\tau_k}\right)\Big/\left(\sum_k\frac{\rho_k}{\tau_k}\right). \tag{8}$$

The total fluid-fluid interaction force at any position $\mathbf{x}$ is given by

$$F_{1k}(x)=-G_c\psi_k(x,t)\sum_i w_i\psi_{\bar{k}}(\mathbf{x}+\mathbf{e}_i\Delta t,t)\mathbf{e}_i, \tag{9}$$

where $\psi_k(x)$ is the effective mass, which is a function of $\mathbf{x}$ through its dependency of density, i.e., $\psi(x,t)=\psi(\rho(x,t))$, and parameter G_c represents the interparticle interactions. The interparticle force of each phase and the solid boundary is defined as

$$F_{2k}(x,t)=-g_{kw}\rho_k(x,t)\sum_i w_i s(\mathbf{x}+\mathbf{e}_i\Delta t)\mathbf{e}_i, \tag{10}$$

where g_{kw} represents the interaction strength between the fluid and the solid and s is an indicator function which is equal to 1 and 0 for solids and fluids, respectively. The interaction strength between the fluid and the solid boundary is adjusted by the parameter g_{kw}. To simulate the hydrophobic and hydrophilic surfaces, g_{kw} is considered positive and negative, respectively. w_i's are the weight coefficients associated with the lattice and, for a D_2Q_9 lattice, have the following values:

$$w_i=\begin{cases}4/9 & i=0\\ 1/9 & i=1,2,3,4\\ 1/36 & i=5,6,7,8.\end{cases} \tag{11}$$

The effect of the gravity can be simply included by considering

$$\mathbf{F}_{3k}=\rho_k\mathbf{g}. \tag{12}$$

Using the Chapman-Enskog expansion, the following continuity and momentum equations can be obtained for the fluid mixture as a single fluid [36,63]:

$$\frac{\partial\rho}{\partial t}+\nabla\cdot(\rho\mathbf{u})=0, \tag{13}$$

$$\rho\left[\frac{\partial\rho}{\partial t}+(\mathbf{u}\cdot\nabla)\mathbf{u}\right]=-\nabla p+\nabla[\mu(\nabla\cdot\mathbf{u}+\mathbf{u}\cdot\nabla)]+\rho\mathbf{F}, \tag{14}$$

where $\rho = \sum_k \rho_k$ is the density of the fluid mixture and the velocity of the fluid mixture is given by $\rho \mathbf{u} = \sum_k \rho_k \mathbf{u}_k + \frac{1}{2}\sum_k \mathbf{F}_k$. F is the total forces exerted on the components.

IV. RESULTS AND DISCUSSION

As depicted in Fig. 1, our simulation domain is a rectangle with a width equal to W and a length equal to L. In all the simulations it is supposed that $\rho_2/\rho_1 = 1$, $\mu_2/\mu_1 = 1$, and $g_{1w} = -g_{2w}$. The values of g_{1w} and g_{2w} are derived from $G_c \cos\theta_E = g_{2w} - g_{1w}$ by keeping θ_E fixed [66]. The parameter G_c determines the surface tension and in this study is considered equal to 1.3. By controlling the parameter g_{1w} we can obtain different contact angles and wettabilities. The contact angle is smaller (larger) than 90° when g_{1w} is negative (positive). In order to solve our problem we, first, calculate the surface tension. The average velocity then is calculated from $u_1 = \rho_1 g h_c^2/3\mu_1$. The capillary number can be determined from $\mathrm{Ca} = \mu_1 u_1/\sigma$.

A. Calculation of the surface tension

The previous LBM studies employ the Laplace's law to calculate the surface tension. Periodic boundary conditions are usually used for all the boundaries in the procedure [66,70]. In the present study we also apply such an approach. We consider a static droplet in a 100 × 100 square box in lattice units and apply the periodic boundary conditions. According to Laplace's law [66], we have

$$p_i - p_o = \frac{\sigma}{R}, \tag{15}$$

where p_i and p_o are the internal and the external pressures of the droplet, respectively, σ represents the surface tension, and R stands for the droplet radius. In order to calculate the pressure from the Laplace's law, the radius of the droplet is determined once the droplet reaches its equilibrium state. The internal and the external pressures are calculated at positions far from the interface because this value changes near the interface [71]. The results are depicted in Fig. 2. The radius of the droplet, the pressure difference, and the surface tension are all in lattice units, which can be conveniently converted to practical values. From Fig. 2 it can be concluded that the slope of the curve, which is equal to the surface tension, is equal to 0.1872.

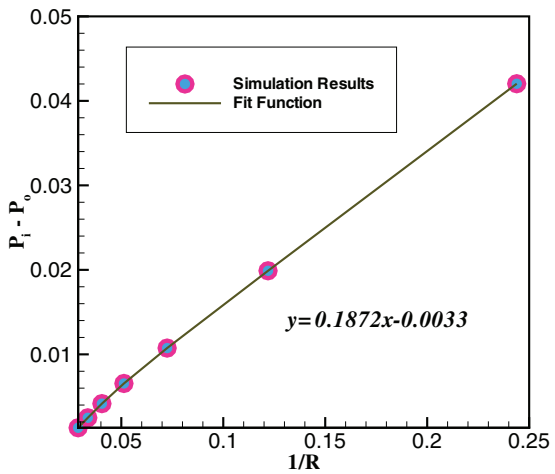

FIG. 2. (Color online) Calculation of the surface tension using the Laplace's law.

B. Numerical verification

In order to verify the numerical results, the LBM results were compared with those obtained using the lubrication theory for a range of capillary numbers and contact angles where the lubrication approximation is valid. Figure 3 depicts the results of the conducted simulations on a plane substrate for $\theta_E = 0°$ and $\mathrm{Ca} = 0.1$. In the lubrication approximation it is assumed that the velocity is unidirectional and is a function of the local height $h(x)$ and its derivative. It can be shown that the height of the film in nondimensional form is given by the following fourth-order differential equation [20]:

$$\frac{\partial h^*}{\partial t^*} = -\vec{\nabla}^* \cdot [h^{*3}\vec{\nabla}^*\vec{\nabla}^{*2}h^* - Ah^{*3}\vec{\nabla}^* h^* + h^{*3}\hat{i}], \tag{16}$$

where $A = (3\mathrm{Ca}^{1/3})\cot(\beta)$ is the only controlling parameter. In the expression for A, β stands for the inclination angle of the substrate. In Eq. (16) the dimensionless parameters are $x^* = x/x_c$ (the gradient terms), $h^* = h/h_c$, and $t^* = t/t_c$, where $x_c = h_c(3\mathrm{Ca})^{-1/3}$ and $t_c = x_c/\bar{u}$. We compare the results with the results of Ref. [72], which considers a slip boundary condition in the above equation. For a plane substrate it is shown that the steady shape of the interface profile can be given by Ref. [20]

$$\frac{\partial^3 h^*}{\partial x^{*3}} = 1 - \frac{1+\zeta}{h^{*2}+\zeta}, \tag{17}$$

where ζ denotes the slip factor. Similarly to Ref. [20], in order to compare the results with the LBM results, the slip parameter and $C = (3\mathrm{Ca})^{-1/3}\tan(\varphi)$ were changed until the best match between the results was achieved. Figure 3 displays the results for $C = 1.536$ and $\zeta = 0.05$. As can be seen, the LBM results are in a very close agreement with those of the lubrication theory. The effect of the spatial discretization on the results is given in the Fig. 3(b) and, as is evident, a 300 × 500 lattice is adequate to study the system.

C. A U-shaped groove

Before considering this case, because of the similarity between the near wall of the U-shaped groove (the first horizontal wall of the groove: see Fig. 1) and the horizontal wall of a right angle wedge, analogously to the work of Ref. [2], we, first, consider the motion of the contact line over a right angle wedge, as depicted in Fig. 4. The fluid 1 has initially occupied a rectangular region and $\mathrm{Ca} = 0.1$ and $\theta_E = 45°$. As the contact line arrives at the corner it gets pinned at this point. Since the inflow rate is constant, an accumulation of the coating material around this region starts to develop [2]. After reaching the height of the capillary ridge to a value large enough for providing the necessary pressure, the contact line moves in the horizontal direction. When the liquid reaches the maximum length that can move along the horizontal wall, the so-called runout length [2], it starts to grow in the vertical direction and drips. As is evident from the figure, the runout

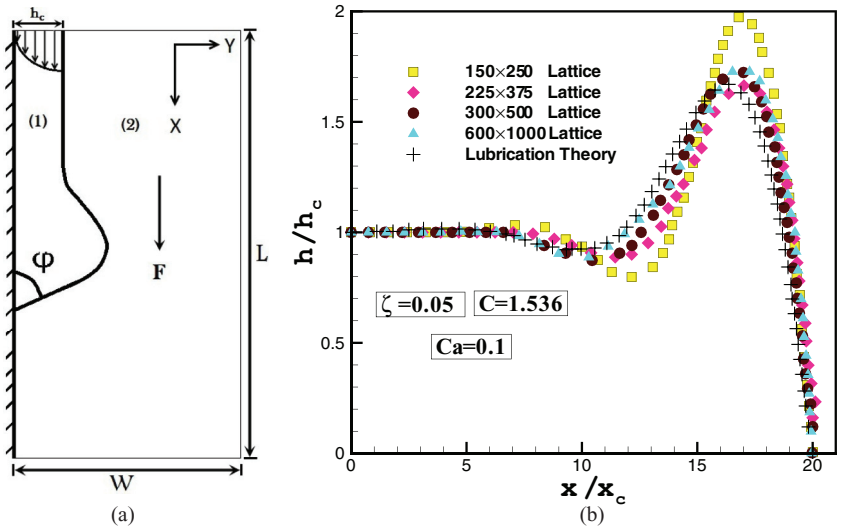

FIG. 3. (Color online) (a) Thin liquid film flow over a plane surface. (b) A comparison between the results of the LBM and the lubrication theory for $\zeta = 0.05$, $C = 1.536$, and $\mathrm{Ca} = 0.1$. The effect of the spatial discretization is shown in the figure.

lengths for $\theta_E = 30^\circ$ and $\mathrm{Ca} = 0.1, 0.15$, and 0.2 are equal to $l_{\max} = 10.68, 7.52$, and 5.46, respectively. This means that by increasing the capillary number the runout length decreases.

Now, let us consider the coating problem over the groove, as depicted in Fig. 5(a). W and L in the simulation domain are equal to 400 and 400, respectively, in lattice units (the units in Fig. 5 and all the following figures are scaled by a factor of 10 in both the x and y directions, namely the units should be multiplied by a factor of 10). We are interested in finding the conditions under which successful coating is possible. It is clear that for deep U-shaped grooves ($D > l_{\max}$) successful coating is not possible because, as already discussed, the drip failure occurs. For narrow grooves, again, successful coating is not possible because the bulge contacts the far wall before

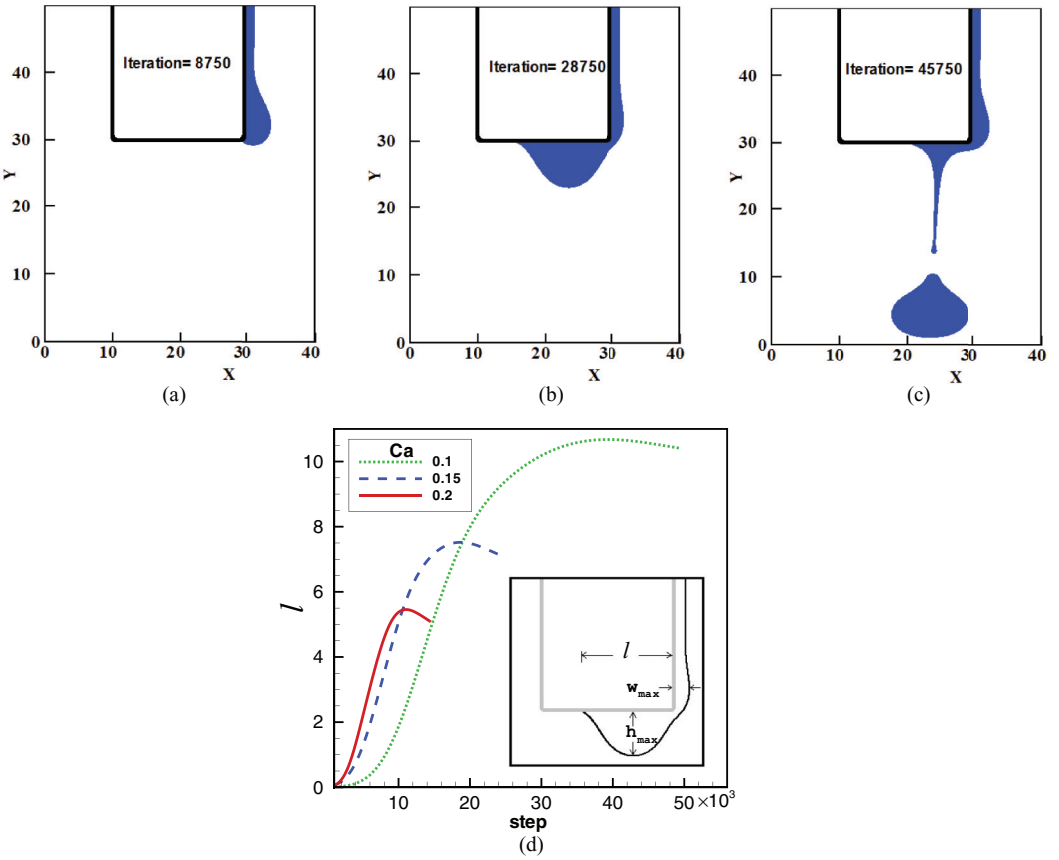

FIG. 4. (Color online) [(a), (b), and (c)] Transient evolution of the moving film over a right angle wedge during different times for $\theta_E = 45^\circ$ and $\mathrm{Ca} = 0.1$. (d) The position of the contact line on the horizontal wall of the right angle wedge as a function of time for $\theta_E = 30^\circ$ and $\mathrm{Ca} = 0.1, 0.15$. and 0.2. The maximum value of the l is the runout length ($l_{\max}$).

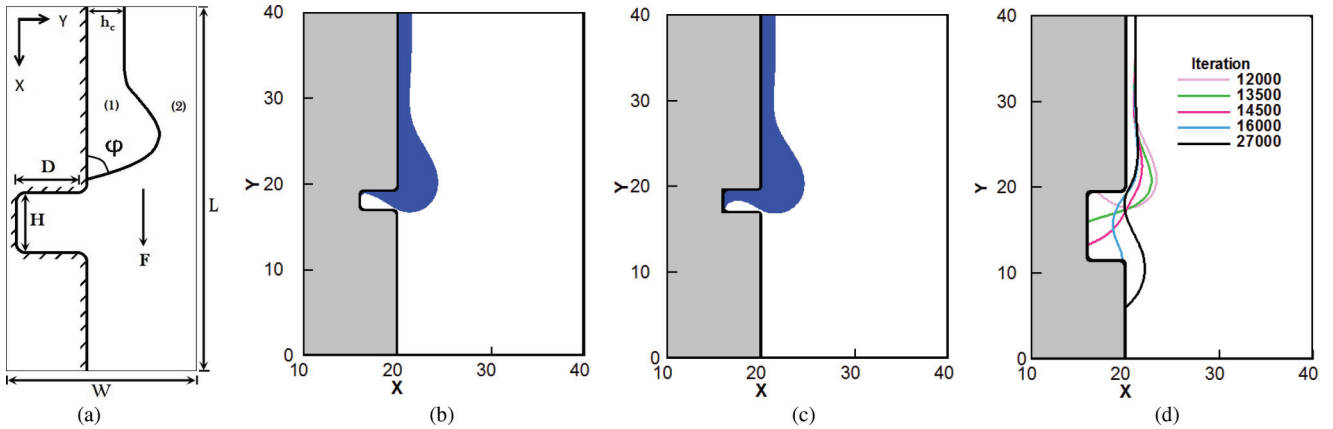

FIG. 5. (Color online) (a) Motion of the contact line over a substrate with a U-shaped groove. (b) A narrow groove ($H = 2.2$) and unsuccessful coating. (c) A wider groove ($H = 2.6$) but the coating is still unsuccessful. (d) Time-dependent evolution of the film during a continuous and successful coating ($H = 8.5$). Ca $= 0.1$, $\theta_E = 30^\circ$, and $D = 4$. The units are scaled by a factor of 10.

reaching the contact line to this wall (capping failure). Based on the groove width, Fig. 5 explains three scenarios that may occur for the groove coating for Ca $= 0.1$ and $\theta_E = 30^\circ$. As displayed in Fig. 5(b) if the groove is very narrow, the bulge contacts the front wall before reaching the contact line to the bottom wall of the groove. Therefore, the coating is not continuous. In Fig. 5(c) the groove is wider than the previous case and the contact line can reach the bottom wall but the bulge still reaches the front wall. In Fig. 5(d) the depth is the same as the cases of Figs. 5(b) and 5(c) but the width is so large that the contact line can surpass the bulge front and the capping problem is removed. It is clear from the above that for a groove with a certain depth, the width should be large enough for successful coating of the groove. These results are in complete agreement with the results of Ref. [2].

Figure 6 depicts the minimum required groove width for successful coating as a function of the depth for Ca $=$ 0.1 and 0.15 and $\theta_E = 30^\circ$ and 45°. Figure 6(b) of the figure indicates that a 400×400 lattice is suitable for this purpose and considering a finer lattice does not change the results appreciably. An examination of Fig. 6 reveals that the minimum required width or the critical width ($H_{\rm cr}$) increases by increasing θ_E for a given value of Ca. These results also are in complete agreement with the results of Ref. [2]. It is seen from Fig. 6 that, for $D \lessapprox 3$, by increasing D the width increases, while for larger values of D the width decreases by increasing D. As the contact line surpasses the bulge, the bulge moves backward and this decreases the critical width by increasing D.

D. A V-shaped groove

Topographical features can be in various shapes. In this section we consider a V-shaped groove as depicted in Fig. 7 and explore geometric conditions under which successful coating is possible for different values of Ca and θ_E. W and L in the

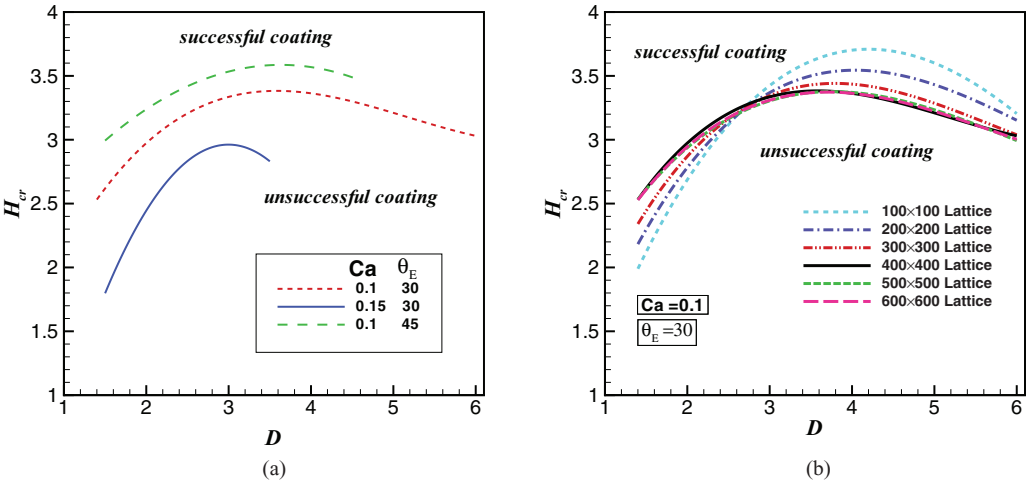

FIG. 6. (Color online) (a) The minimum required width ($H_{\rm cr}$) for successful coating of a U-shaped groove as a function of the groove depth (D) for different values of the capillary number (Ca) and the contact angle (θ). (b) the effect of the spatial discretization on the results. The units are scaled by a factor of 10.

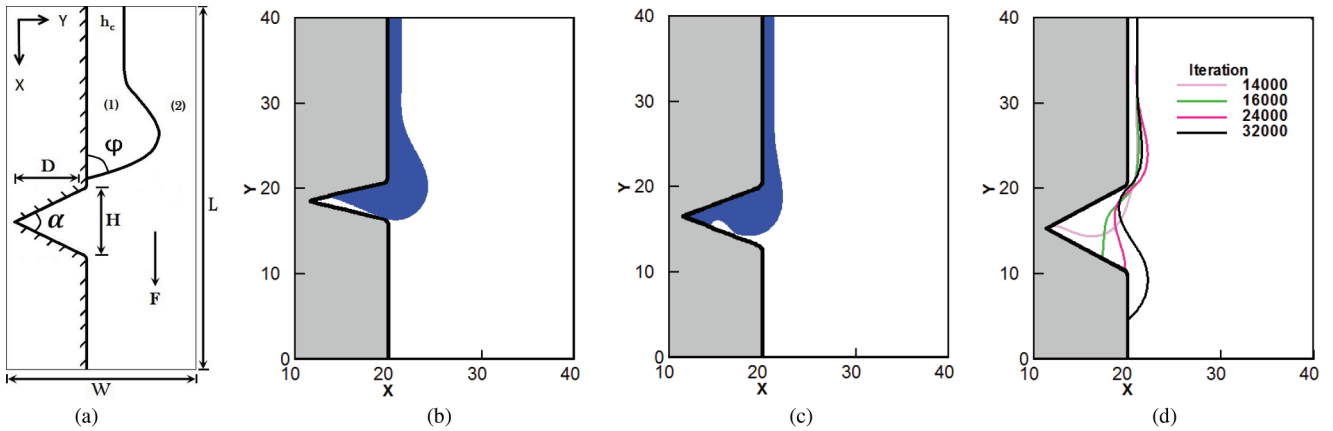

FIG. 7. (Color online) (a) Motion of the contact line over a V-shaped groove. The height and the width of the groove are D and H, respectively. The groove angle $\tan(\alpha) = H/2D$ is also shown in the figure. (b) The groove angle α is very small ($H = 5.5$, $\alpha = 34.7^\circ$) and the coating is not successful. (c) α is larger ($H = 8.2$, $\alpha = 49.96^\circ$) compared to the previous case but the coating is not successful. (d) The width and groove angle ($H = 11.5$, $\alpha = 66.32^\circ$) are greater than the critical groove angle and coating is successful. Ca $= 0.1$, $\theta_E = 30^\circ$, and $D = 8.8$ for all the cases considered. The units are scaled by a factor of 10.

simulation domain are equal to 400 and 400, respectively, in lattice units. For a V-shaped groove, the important geometric parameters are height H, width D (all scaled with h_c), and groove angle α. The groove angle is related to H and D via $\tan(\alpha/2) = H/(2D)$. As illustrated in Fig. 7 for a V-shaped groove with a fixed depth, successful coating is not possible for all the widths H. As is evident in Fig. 7(b), if H is small, the value of α will be small and the bulge contacts the front wall of the groove before the contact line can reach this wall and this results in noncontinuous coating. Noncontinuous coating may occur even if the contact line can reach the front wall of the groove [see Fig. 7(c)]. Figure 7(d) explains that by increasing α from a certain value (α_{cr}) the coating becomes continuous. Figure 8 represents the critical groove angle (α_{cr}) as a function of depth for Ca $= 0.1$ and 0.15 and $\theta_E = 30^\circ$ and 45°. As depicted in Fig. 8(b), a 400×400 lattice can predict the critical width well. Based on these results, it can be concluded that the α_{cr} increases by increasing Ca and θ_E. Moreover, for $D \lessapprox 4$, by increasing D the critical groove angle (α_{cr}) for continuous coating increases. However, for $D \gtrapprox 4$, α_{cr} decreases by increasing D.

It should be noted that although for $\alpha > \alpha_{cr}$ the contact line can reach all the points over the surface of the groove and the coating is continuous, when the contact angle exceeds a value, the groove is not completely filled with the coating material. Therefore, there is a maximum groove angle for which the groove is completely filled and the coating is successful. Our results suggest that the coating is continuous and the groove is filled completely as long as $\alpha_{cr} \leqslant \alpha \leqslant 1.3\alpha_{cr}$.

E. Two U-shaped grooves

As depicted in Fig. 1(a), we consider surface coating of the substrates with two U-shaped grooves. W and L in the simulation domain are considered equal to 300 and 600, respectively. From the results of the previous sections we can determine the critical dimensions for the successful coating of the first groove for given values of Ca and θ_E. For the second

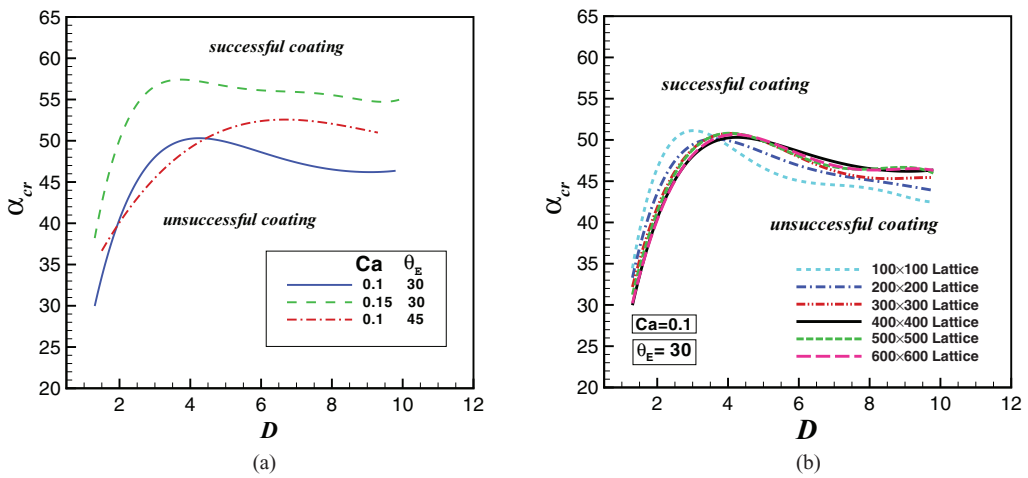

FIG. 8. (Color online) (a) The critical contact angle for a successful coating of a V-shaped groove as a function of the groove depth for different values of Ca and θ_E. (b) The effect of the spatial discretization on the results. The units are scaled by a factor of 10.

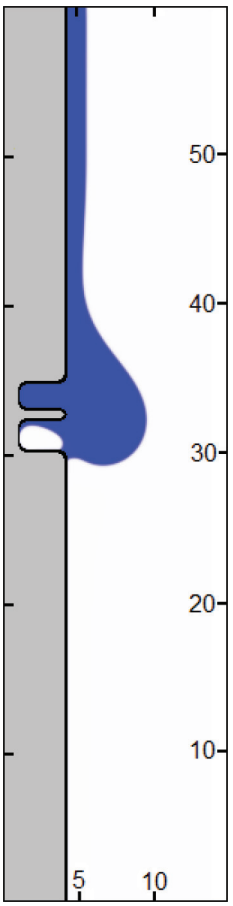

FIG. 9. (Color online) The selected strategy to determine the critical width of the second groove for successful coating. The second groove is considered very close to the first one and the width of the second groove is increased until the whole area of the second groove is filled with the coating material. For the shown case $D_1 = D_2 = 3.2$, $H_1 = 1.6$, and $H_2 = 1.9$. The critical height for the second groove is equal to 2. The units are scaled by a factor of 10.

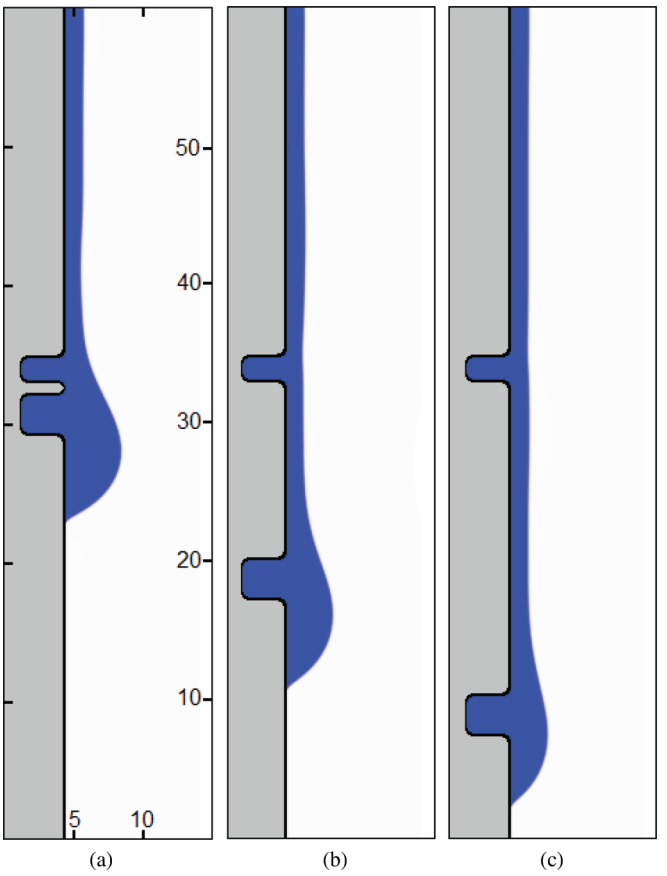

FIG. 10. (Color online) Continuous coating of the second groove when the width of the second groove ($H_2 = 2.6$) is greater than the critical width ($H_{2,\mathrm{cr}} = 2.0$). In this condition continuous coating does not depend on the distance between the grooves and for any distance [cases (a), (b), and (c)] the coating will be continuous. For the cases shown, $\theta_E = 5^\circ$, Ca $= 0.1$, and $D_1 = D_2 = 3.2$. The units are scaled by a factor of 10 and are shown only for the first case (a).

groove we suppose that the depth of the groove is fixed equal to the depth of the first groove ($D_2 = D_1$) and concentrate our attention on finding the width of the groove such that the coating is successful.

As explained in Fig. 9, the dynamic contact angle obtains its maximum value just after leaving the first groove. For the considered case $\theta_E = 5^\circ$ and Ca $= 0.1$. The depths of the groove are equal to 3.2. The critical width for the first groove is equal to 1.6. Clearly, the coating over the second groove will not be successful if the width of the second groove is smaller than the critical width of the first groove, independent of the distance between the grooves. The capping and drip failures will happen over the second groove if the distance between the grooves is small and the width of the second groove is equal to this critical width. Because of the small distance between the grooves the ridge does not have enough time to recover its configuration before entering the first groove and the dynamic contact angle remains not suitable for successful coating.

Now, as illustrated in Fig. 9, let us consider the second groove in a very close distance of the first groove and increase the width until the minimum width for which the coating is successful is achieved. If the width of the second groove is considered equal to this size, the second groove always will be coated successfully, independent of the distance between the grooves (see Fig. 10) because the ridge recovers its initial profile and the dynamic contact angle gradually reduces and reaches to its value before entering the first groove. We call this width the critical width of the second groove ($H_{2,\mathrm{cr}}$). If the width of the second groove is considered between the critical widths of the first and the second grooves, continuous coating of the second groove will be possible only if the second groove is in a certain distance (critical distance) from the first groove. This distance is required to provide a suitable dynamic contact angle for successful coating. Otherwise the coating will be noncontinuous (see Fig. 11).

Our results indicate that, similarly to the critical width of the first groove, the critical width of the second groove is a function of Ca and θ_E. In Table I the critical widths are given for different values of Ca and θ_E. For a constant Ca (contact angle), since the contact angle (Ca) changes, the critical widths of the first and the second grooves change accordingly. One should also change the depth of the grooves to prevent drip failure for successful coating. In order to have a comparison between the critical distances, we reduce the width of the second groove to $H_{2,\mathrm{cr}} - 0.1$ for all the cases mentioned in

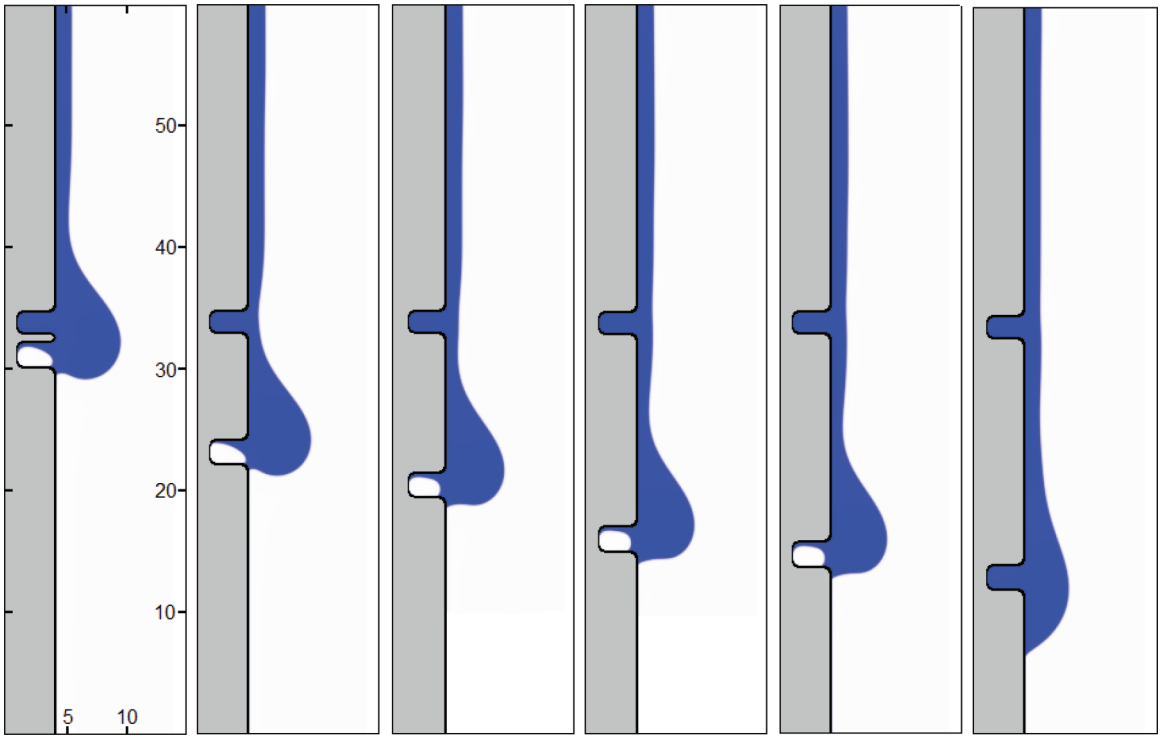

FIG. 11. (Color online) The existence of the critical distance between two U-shaped grooves for successful coating. The width of the second groove ($H_2 = 1.9$) is less than the critical width for the second groove, $H_{2,cr} = 2.0$. From (a) to (f) the distance between the grooves is increased. For the cases (a)–(e) the coating is not continuous and a part of the second fluid (white color) is trapped below the coating film as the bulge meets the far wall of the second groove. For the case (f) the distance between the grooves is equal to the critical distance ($L_c = 18.1$) and the coating is continuous. For the shown case $\theta_E = 5^\circ$, Ca $= 0.1$ and $D_1 = D_2 = 3.2$. The units are scaled by a factor of 10 and are shown only for (a).

Table I and then calculate the critical distance for this width. As depicted in Fig. 12(a) the critical distance between the two grooves may decrease or increase as a function of the contact angle for a given Ca. For Ca $= 0.1$ the critical distance decreases by increasing the contact angle when $\theta_E < 10^\circ$ and increases by increasing the contact angle when $\theta_E > 10^\circ$. Also, as is evident from Fig. 12(b) for $\theta_E = 10$ and different values of Ca, the critical distance between the grooves decreases by increasing Ca when Ca < 0.1 and increases by increasing Ca when Ca > 0.1. In other words, at $\theta_E \approx 15$ and Ca ≈ 0.1 the system behavior alters and the slope of the curve changes its sign. In order to determine the critical distance between two grooves, since the results may depend on the number of the lattices that are located in the grooves, we compared the results for different lattice numbers. The results have also been shown in Fig. 12. As can be seen by increasing the lattice numbers from 300×600, the changes in the results for both cases are negligible.

TABLE I. The critical widths for the first and the second grooves for the case with two U-shaped grooves for various values of the capillary number and the contact angle.

Ca $= 0.1$				$\theta_E = 10^\circ$			
θ_E	$D_1 = D_2$	$H_{1,cr}$	$H_{2,cr}$	Ca	$D_1 = D_2$	$H_{1,cr}$	$H_{2,cr}$
0°	3.2	1.5	1.9	0.05	3.2	1.2	1.4
5°	3.2	1.6	2.0	0.075	2.8	1.2	1.4
10°	3.2	1.7	2.1	0.1	3.2	1.7	2.1
15°	3.4	1.9	2.2	0.125	3.1	1.9	2.3
20°	3.4	2	2.3	0.15	2.7	1.9	2.4
25°	3.2	2.3	2.3	0.175	2.3	1.7	2.0
30°	3.1	2.5	2.4	0.2	2	1.3	1.9

It has been shown that by increasing Ca the capillary height decreases [65]. Therefore, for small values of Ca (Ca $= 0.05$), the capillary height is very large. This results in accumulation of a considerable amount of fluid during the coating of the first groove as displayed in Fig. 13(a). This creates a large value for the dynamic contact angle after leaving the contact line from the first groove [see Fig. 13(b)]. Therefore, the film should travel a large distance to reach a suitable dynamic contact angle to coat the second groove successfully. For this reason, for Ca < 0.1, by increasing the capillary number, the critical distance decreases due to the decrease of the capillary height but for Ca > 0.1 the critical distance increases despite the decrease of the capillary height. Our results indicate that for Ca > 0.1 the effect of increasing Ca on the dynamic contact angle [65] is more than the effect of decreasing the capillary height and, in total, the dynamic contact angle increases. As the dynamic contact angle increases, the fluid film should travel a larger distance to reach a suitable dynamic contact angle

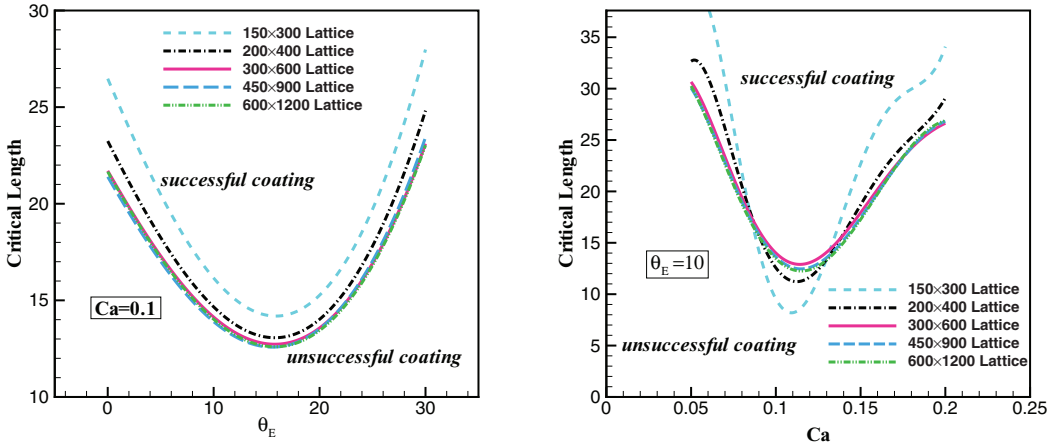

FIG. 12. (Color online) The effect of Ca and θ_E on the critical distance. (a) Ca = 0.1 and different values of the contact angle and (b) $\theta_E = 10^\circ$ and different values of Ca. The effect of the lattice numbers on the results have been shown. The units are scaled by a factor of 10.

for suitable coating of the second groove. Due to this, by increasing Ca, the critical distance increases for Ca > 0.1. A similar situation occurs for the case when the capillary number is fixed and the contact angle changes.

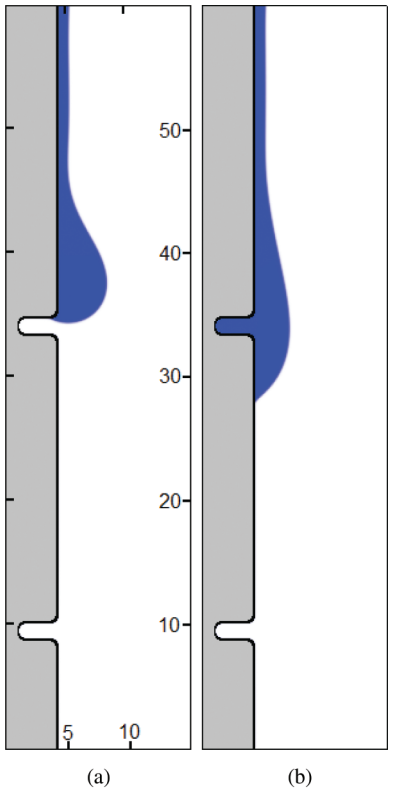

FIG. 13. (Color online) The effect of increasing the capillary height for a substrate with two U-shaped grooves. The width of the second groove is equal to that of the first groove $H_2 = 1.8$ (less than the critical width for the second groove, $H_{2,cr} = 2.1$, in lattice units). For the shown cases Ca = 0.1 and $\theta_E = 10^\circ$. (a) The capillary height increases before entering the film into the first groove. (b) The first groove is coated with the material of the film. The units are scaled by a factor of 10 and the units are shown only for (a).

In coating problems it is important to study the effects of the viscosity and the density ratios. It is known that the multicomponent Shan-Chen model is prone to numerical instabilities when the viscosity or density ratios differ from 1. By increasing these ratios the numerical instabilities grow. However, the method has shown its capabilities in capturing essential physics of many systems and problems such as dynamical systems [37], micro- and nanosystems [59–61], capillary imbibition [62], capillary filling [63], and nonideal fluids in confined geometries [64]. Despite the restrictions, we were able to simulate the system for density and viscosity ratios differing from 1, although close to it. Figures 14 and 15 illustrate the differences between the results of the case with $\rho_2/\rho_1 = 2$ and $\mu_2/\mu_1 = 6$ ($\rho_2 = 1, \rho_1 = 0.5$,

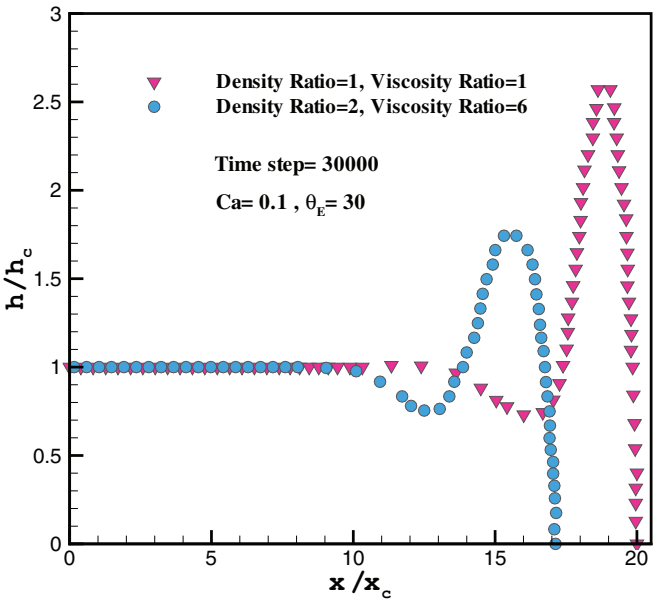

FIG. 14. (Color online) The effect of the viscosity and density ratios on the dynamics and the ridge profile for a film over a smooth surface. Ca = 0.1, $\theta_E = 30^\circ$, and the time step is equal to 30 000 for both cases. The units are scaled by a factor of 10.

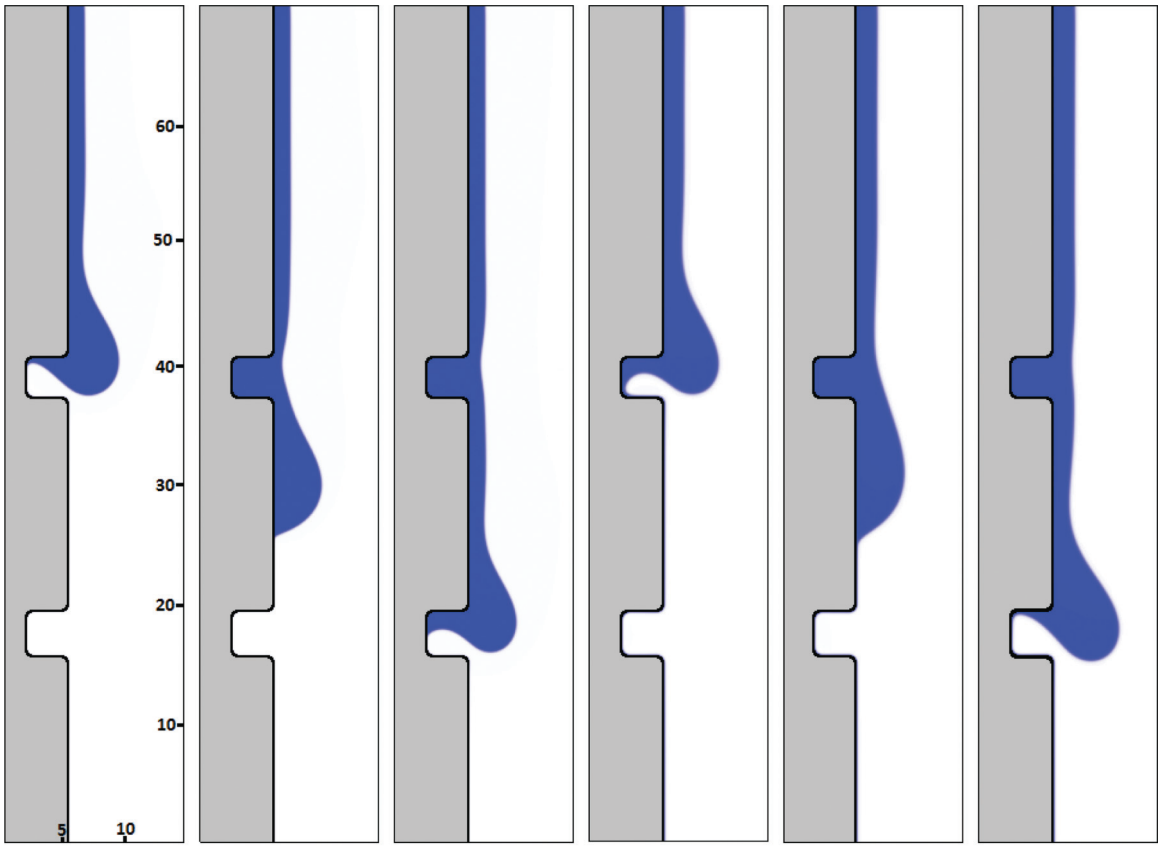

FIG. 15. (Color online) The effect of the viscosity and the density ratios on the coating procedure. Panels (a), (b), and (c) belong to the case with the same viscosities and densities and panels (e), (f), and (g) belong to the case with $\rho_2/\rho_1 = 2$ and $\mu_2/\mu_1 = 6$. The time steps for the panels (a) to (g) are 7000, 11 000, 15 000, 10 000, 16 000, and 21 000, respectively. For all the cases considered Ca $= 0.1$ and $\theta_E = 10^\circ$. The units are scaled by a factor of 10 and the units are shown only for (a).

$\tau_2 = 1.248, \tau_1 = 0.752$) and the case with the same densities and viscosities. Figure 14 reveals that, for the case of steady-state film flow over a smooth surface, by increasing the viscosity and density ratios, the dynamics is weakened and the ridge profile is flattened. Figure 15 shows that the coating procedure is affected qualitatively when the viscosity and density ratios are increased. However, the available results do not support a more substantial conclusion and to get deeper insight into the case further investigation is required. Nevertheless, one may anticipate some differences in the results if a liquid-vapor or liquid-gas system is used instead of the current liquid-liquid system. One of the main differences may appear in the blocking of the vapor or gas phase in the groove (capping failure). While for the liquid-liquid case the trapped liquid is expected to remain blocked, the isolated vapor or gas phase may possibly move away from the groove into the contiguous liquid phase area, particularly for small contact angles. For the vapor case condensation also may occur.

F. Two V-shaped grooves

Our strategy in determining the dimensions for the case with two V-shaped grooves is the same as described for the case with two U-shaped grooves. We, first, obtain the critical width (groove angle) of the first groove for given values of the equilibrium contact angle and the capillary number such that for smaller widths (groove angles) the coating is not successful. In determining the dimensions of the second groove we consider the depth of the second groove equal to that of the first and find the minimum width of the groove such that for smaller values of the width the coating is not continuous. Table II reports the calculated critical widths for different values of Ca and θ_E.

TABLE II. The critical widths for the first and second grooves for the case with two V-shaped grooves for various values of the capillary number and contact angle.

Ca $= 0.1$				$\theta_E = 10^\circ$			
θ_E	$D_1 = D_2$	$H_{1,\mathrm{cr}}$	$H_{2,\mathrm{cr}}$	Ca	$D_1 = D_2$	$H_{1,\mathrm{cr}}$	$H_{2,\mathrm{cr}}$
0°	3.4	2.8	3.0	0.05	3.4	2.1	2.3
5°	3.5	3.0	3.2	0.075	3.6	3.1	3.3
10°	3.5	3.1	3.3	0.1	3.5	3.1	3.3
15°	3.7	3.2	3.4	0.125	3.4	3.1	3.3
20°	3.8	3.5	3.5	0.15	3.5	3.4	3.6
25°	3.9	3.6	3.6	0.175	3.6	3.5	3.8
30°	3.9	3.9	3.6	0.2	3.6	3.9	4.6

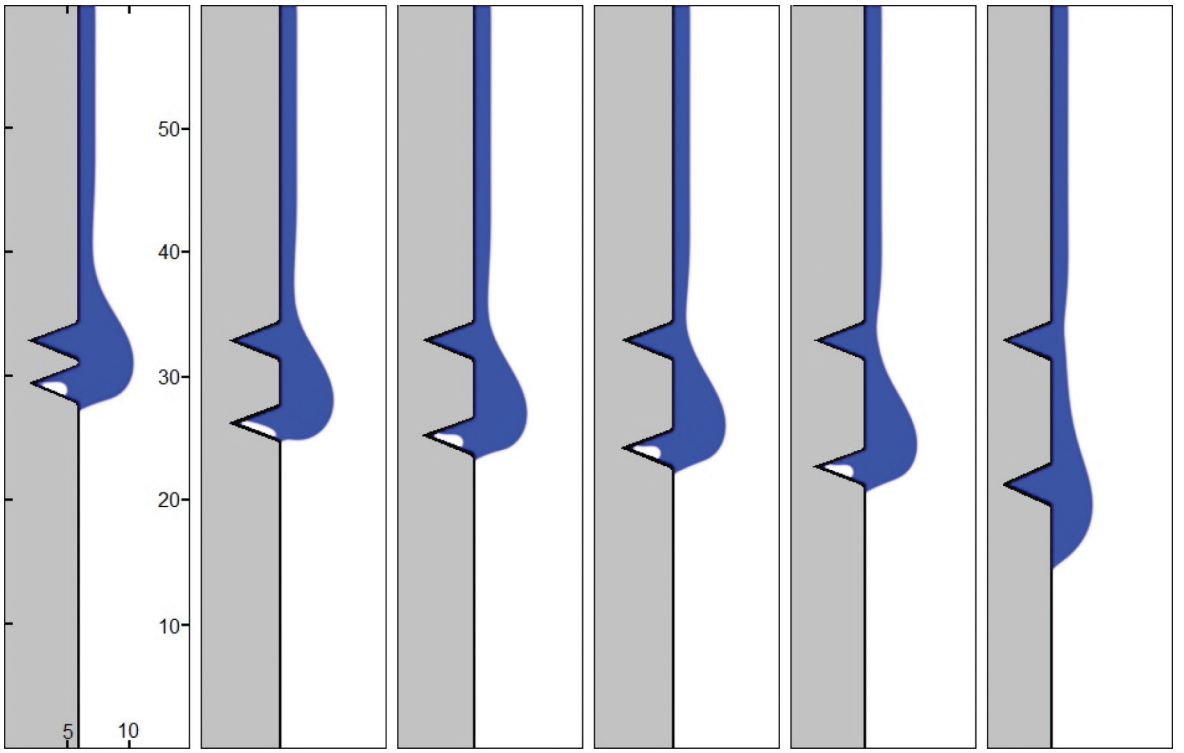

FIG. 16. (Color online) The existence of the critical distance between two V-shaped grooves for successful coating. The width $H_2 = 3.1$ (groove angle $\alpha_2 = 47.73^\circ$) of the second groove is less than the critical width $H_c = 3.2$ (groove angle $\alpha_c = 49.13^\circ$). From (a) to (f) the distance between the grooves is increased. For the cases (a)–(e) the coating is not continuous and a part of the second fluid (white color) is trapped below the coating film as the bulge meets the far wall of the second groove. For case (f) the distance between the grooves is equal to the critical distance $L_c = 9.4$ and the coating is continuous. For the shown cases $\theta_E = 5^\circ$, Ca $= 0.1$, $H_1 = 3$, and $D_1 = D_2 = 3.5$. The units are scaled by a factor of 10 and the units are shown only for (a).

As depicted in Fig. 16 our results indicate that there is a critical distance between the grooves when the width of the second is a value between the critical widths and continuous surface coating is possible only if the distance between the grooves is not smaller than this certain distance. Applying the procedure described in Fig. 16, we calculated the critical distance for different values of Ca and θ_E given in Table II. The results are presented in Fig. 17. As is evident from Fig. 17(a), the critical distance between two grooves for Ca $= 0.1$ decreases by increasing the contact angle when $\theta_E < 10$ and increases by increasing the contact angle when $\theta_E > 10$. Also from Fig. 17(b) it can be observed that for

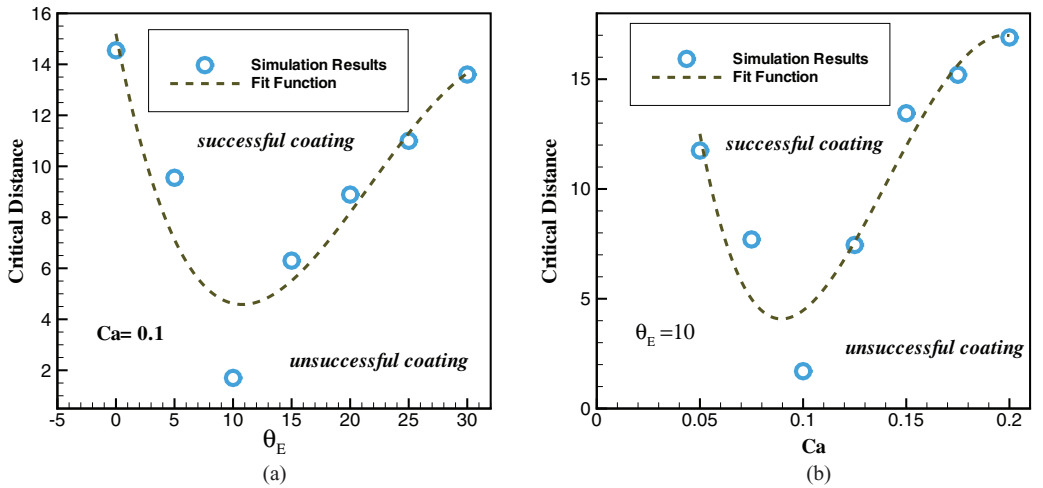

FIG. 17. (Color online) The effect of Ca and θ_E on the critical distance for a substrate with two V-shaped grooves. The results are for (a) Ca $= 0.1$ and different values of the contact angle and (b) $\theta_E = 10^\circ$ and different values of Ca. The units are scaled by a factor of 10.

TABLE III. The geometric parameters and the critical width for the groove for the case with a mound and a U-shaped groove for various values of the capillary number and the contact angle.

Ca = 0.1				$\theta_E = 10^\circ$			
θ_E	$D_1 = D_2$	H_1	$H_{2,\mathrm{cr}}$	Ca	$D_1 = D_2$	H_1	$H_{2,\mathrm{cr}}$
0°	3.0	1.8	1.6	0.05	3.0	1.8	1.1
5°	3.0	1.8	1.7	0.075	3.0	1.8	1.3
10°	3.0	1.8	1.8	0.1	3.0	1.8	1.8
15°	3.0	1.8	1.9	0.125	3.0	1.8	1.9
20°	3.0	1.8	2.0	0.15	3.0	1.8	2.1
25°	3.0	1.8	2.1	0.175	3.0	1.8	2.4
30°	3.0	1.8	2.2	0.2	3.0	1.8	2.7

$\theta_E = 10$ the critical distance between the grooves decreases by increasing Ca when Ca < 0.1 and increases by increasing Ca when Ca > 0.1.

G. A mound and a groove

In order to check the effects of locating a mound before a groove on the coating process we consider a driven liquid film over a substrate with a mound and a U-shaped groove, as depicted in Fig. 1(b). W and L in the simulation domain are equal to 300 and 700, respectively. For our purpose we keep the height and the width of the mound almost equal to the average widths and depths of the already considered cases, namely, $D_1 = 3$ and $H_1 = 1.8$, for all the cases considered.

Similarly to the previous sections, our results imply that there is a critical width for the groove (see Table III). Moreover, if the groove width lies between the critical widths without and with the mound, continuous surface coating is not possible for an arbitrary distance between the mound and the groove. Figure 18 illustrates that, based on the value of Ca and θ_E, there is a critical distance such that for distances between the mound and the groove that are larger than this distance, continuous coating is possible and, for smaller distances, coating is not successful. Figure 19 depicts the critical distance between the mound and the groove for a given capillary number (Ca = 0.1) and different values of the contact angle and also for a given contact angle ($\theta_E = 10^\circ$) and different values of the capillary number. As is evident from the figure, for $\theta_E < 20^\circ$ (Ca < 0.075), by increasing θ_E (Ca), the critical distance decreases and for the other region the critical distance increases by increasing the θ_E. As already discussed, this behavior is due to the increase of the dynamic contact angle that arises because of increasing the capillary height or the static contact angle.

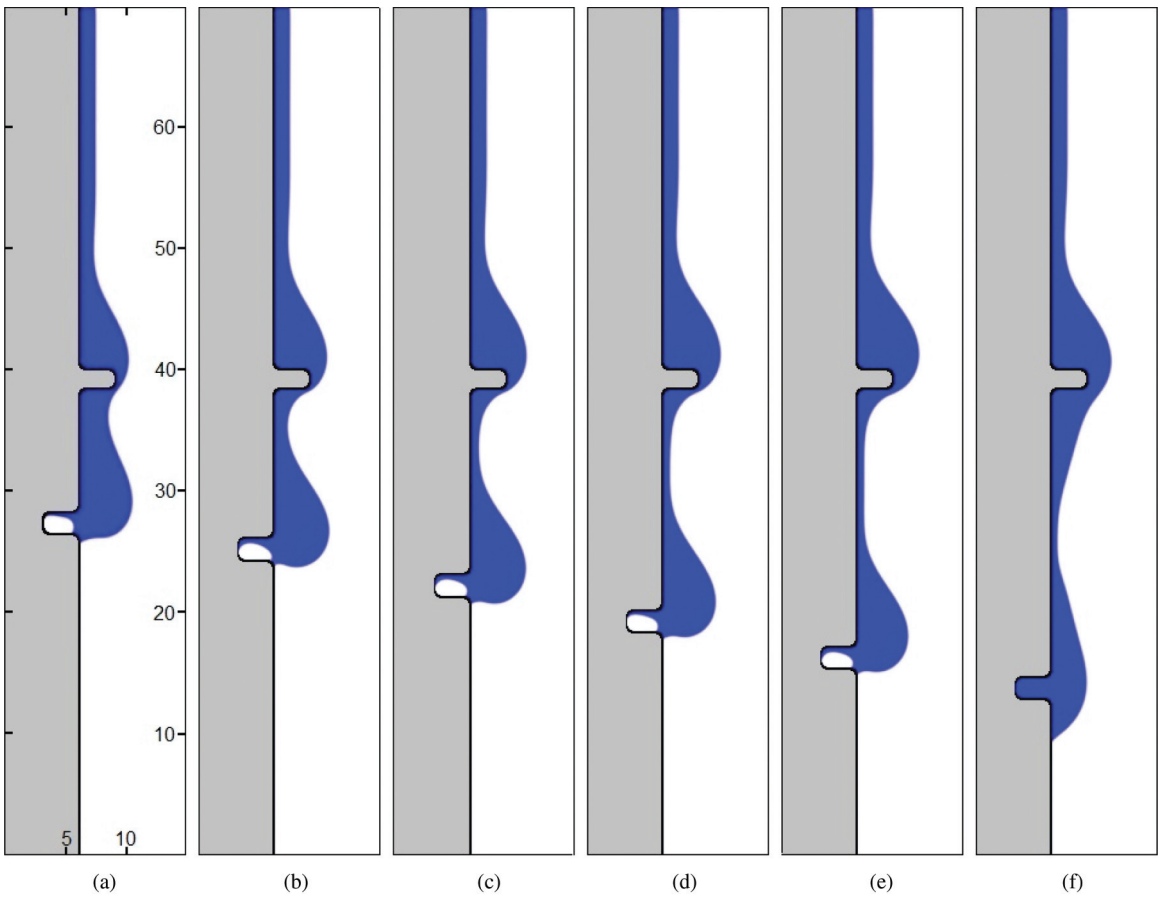

FIG. 18. (Color online) There is a critical distance between the mound and the groove such that for distances smaller than it the coating is not continuous [cases (a)–(e)]. As can be seen, by increasing the distance to $L_c = 21.3$ the substrate is finally coated successfully [case (f)]. For the cases shown Ca = 0.1, $\theta_E = 5^\circ$ and the critical width for the groove is 1.7. The units are scaled by a factor of 10 and the units are shown only for (a).

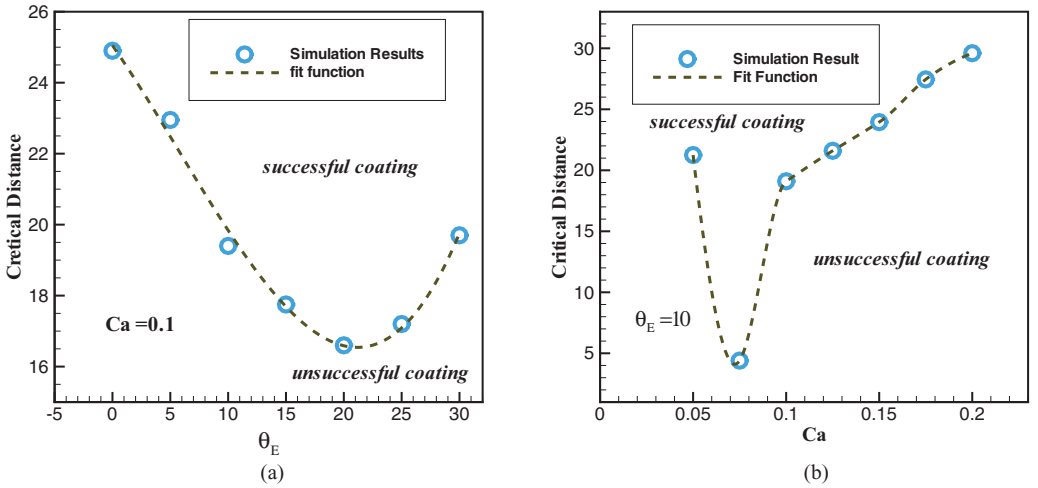

FIG. 19. (Color online) The effect of the contact angle and the capillary number on the critical distance for the case of a substrate with a mound and a U-shaped groove. The results are for (a) Ca = 0.1 and different values of the contact angle and (b) $\theta_E = 10^\circ$ and different values of Ca.The units are scaled by a factor of 10.

V. CONCLUSION

We employed a multicomponent lattice Boltzmann scheme and investigated the dynamics of gravity-driven thin liquid films over topographically textured surfaces. For a surface with a U-shaped groove it was shown that there are certain conditions under which the coating is not successful. For a given capillary number, contact angle, and depth of the groove, there is a critical width such that, if the groove width exceeds this critical value, the coating is successful. These results were in complete agreement with the available results [2,65]. For a V-shaped-type groove our investigation revealed that there is no runout length. Because of the direction of gravity, the contact line continues its motion over the inclined face and drip failure does not occur. If the groove angle is smaller than a certain critical value (α_{cr}), capping failure may occur. Moreover, if the groove angle is very large ($\alpha > 1.3\alpha_{cr}$), the groove is not filled completely by the material of the coating layer. For a definite groove height, the critical contact angle depends on the contact angle and the capillary number.

Our results revealed that the presence of a topographical feature such as a groove or a mound imposes more difficult conditions on successful coating of the subsequent grooves. This means that the required conditions for coating of the substrates with many topographical features can differ completely from those understood for the substrates with a single topographical feature.

For substrates with two grooves, based on the values of Ca and θ_E, there is a critical width for the second groove, which is larger than the critical width of the first groove. If the width of the second groove is larger than the critical width, the coating will be successful independent of the distance between the grooves. However, if the width of the second groove is smaller than this critical width and larger than the critical width of the first groove, there is a critical distance between the grooves such that, for a distance smaller than the critical distance, the coating of the second groove is not continuous. Our results showed that for a given contact angle (capillary number) the critical distance is a convex function of the capillary number and it is large for both the small and large capillary numbers (contact angles). For large capillary numbers, the dynamic contact angle is large and this increases the critical distance. For small capillary numbers, the capillary height is large and this increases the dynamic contact angle just after leaving the contact line from the first groove and, as a result, the critical distance increases.

Our investigation showed that the presence of a mound also makes the coating conditions more restrictive and similar results to those with two grooves may be obtained for the cases with a mound and a groove.

[1] H. C. Ko, M. P. Stoykovich, J. Song, V. Malyarchuk, W. M. Choi, C.-J. Yu, J. B. Geddes, J. Xiao, Y. Huang, and J. A. A. Rogers, Nature **454**, 748 (2008).
[2] G. M. Gramlich, A. Mazouchi, and G. M. Homsy, Phys. Fluids **16**, 1660 (2004).
[3] S. Veremieiev, H. M. Thompson, Y. C. Lee, and P. H. Gaskell, Chem. Eng. Process. **50**, 537 (2011).
[4] A. Moosavi, M. Rauscher, and S. Dietrich, Phys. Rev. Lett. **97**, 236101 (2006).
[5] M. M. J. Decré and J.-C. Baret, J. Fluid Mech. **487**, 147 (2003).
[6] S. J. Baxter, H. Power, K. A. Cliffe, and S. Hibberd, Phys. Fluids **21**, 032102 (2009).
[7] K. Helbig, R. Nasarek, T. Gambaryan-Roisman, and P. Stephan, J. Heat Trans. **131**, 011601 (2009).
[8] H. Yu, K. Löffler, T. Gambaryan-Roisman, and P. Stephan, Comput. Thermal Sci. **2**, 455 (2010).
[9] E. Dressaire, L. Courbin, J. Crest, and H. A. Stone, Phys. Rev. Lett. **102**, 194503 (2009).
[10] A. Alexeev, T. Gambaryan-Roisman, and P. Stephan, Phys. Fluids **17**, 062106 (2005).
[11] M. P. Brenner, Phys. Rev. E **47**, 4597 (1993).

[12] L. W. Schwartz, Phys. Fluids A **1**, 443 (1989).
[13] D. T. Moyle, M.-S. Chen, and G. M. Homsy, Int. J. Multiphase Flow **25**, 1243 (1999).
[14] Jin Liu, Moran Wang, Shiyi Chen, and Mark O. Robbins, Phys. Rev. Lett. **108**, 216101 (2012).
[15] P. H. Gaskell, P. K. Jimack, M. Sellier, and H. M. Thompson, Phys. Fluids **18**, 013601 (2006).
[16] S. Kalliadasis, C. Bielarz, and G. M. Homsy, Phys. Fluids **12**, 1889 (2000).
[17] M. Scholle, A. Haas, N. Aksel, M. C. T. Wilson, H. M. Thompson, and P. H. Gaskell, Phys. Fluids **20**, 123101 (2008).
[18] M. R. Sadigh, T. Gambaryan-Roisman, and P. Stephan, Phys. Fluids **24**, 014104 (2012).
[19] M. R. Wang, J. K. Wang, and S. Y. Chen, J. Comput. Phys. **226**, 836 (2007).
[20] R. Ledesma-Aguilar, A. Hernández-Machado, and I. Pagonabarraga, Phys. Fluids **20**, 072101 (2008).
[21] R. Ledesma-Aguilar, A. Hernández-Machado, and I. Pagonabarraga, Soft Matter **7**, 6051 (2011).
[22] R. Ledesma-Aguilar, A. Hernández-Machado, and I. Pagonabarraga, Langmuir **26**, 3292 (2010).
[23] A. Dupuis and J. M. Yeomans, Langmuir **12**, 2624 (2005).
[24] A. Dupuis and J. M. Yeomans, Europhys. Lett. **75**, 105 (2006).
[25] F. Varnik, M. Gross, N. Moradi, G. Zikos, P. Uhlmann, P. M. P. Müller-Buschbaum, D. Magerl, D. Raabe, I. Steinbach, and M. Stamm, J. Phys.: Condens. Matter **23**, 184112 (2011).
[26] J. J. Huang, C. Shu, and Y. T. Chew, Phys. Fluids **21**, 022103 (2009).
[27] J. Hyväluoma, C. Kunert, and J. Harting, J. Phys.: Condens. Matter **23**, 184106 (2011).
[28] J. J. Huang, C. Shu, and Y. T. Chew, J. Colloid Interf. Sci. **328**, 124 (2008).
[29] J. Hyväluoma, P. Raiskinmäki, A. Jäsberg, A. Koponen, M. Kataja, and J. Timonen, Phys. Rev. E **73**, 036705 (2006).
[30] S. Chibbaro, E. Costa, D. I. Dimitrov, F. Diotallevi, A. Milchev, D. Palmieri, G. Pontrelli, and S. Succi, Langmuir **25**, 12653 (2009).
[31] S. Succi, *The Lattice Boltzmann Equation: For Fluid Dynamics and Beyond* (Oxford University Press, New York, 2001).
[32] M. Cieplak, Phys. Rev. E **51**, 4353 (1995).
[33] G. D. Goolen, *Lattice Gas Methods for Partial Differential Equations* (Addison-Wesley, Reading, Massachusetts, USA, 1989).
[34] A. K. Gunstensen, D. H. Rothman, S. Zaleski, and G. Zanetti, Phys. Rev. A **43**, 4320 (1991).
[35] X. Shan and H. Chen, Phys. Rev. E **47**, 1815 (1993).
[36] X. Shan and G. D. Doolen, Phys. Rev. E **54**, 3614 (1996).
[37] X. Shan and G. D. Doolen, J. Stat. Phys. **81**, 379 (1995).
[38] X. Shan and H. Chen, Phys. Rev. E **49**, 2941 (1994).
[39] Q. Kang, D. Zhang, and S. Chen, Phys. Fluids **14**, 3203 (2002).
[40] M. Swift, S. Orlandini, W. Osborn, and J. Yeomans, Phys. Rev. E **54**, 5041 (1996).
[41] S. Chen and G. D. Doolen, Ann. Rev. Fluid Mech. **30**, 329 (1998).
[42] M. Latva-Kokko and D. H. Rothman, Phys. Rev. E **71**, 056702 (2005).
[43] I. Halliday, A. P. Hollis, and C. M. Care, Phys. Rev. E **76**, 026708 (2007).
[44] T. J. Spencer, I. Halliday, and C. M. Care, Phil. Trans. R. Soc. A **369**, 2255 (2011).
[45] L. O. E. Santos, P. C. Facin, and P. C. Philippi, Phys. Rev. E **68**, 056302 (2003).
[46] F. G. Wolf, L. O. E. dos Santos, and P. C. Philippi, Microfluid Nanofluid **4**, 307 (2008).
[47] F. G. Wolf, L. O. E. dos Santos, and P. C. Philippi, J. Stat. Mech. (2009) P06008.
[48] R. Zhang, Ph.D. thesis, University of Delaware, 1999.
[49] D. J. Holdych, D. Rovas, J. G. Georgiadis, and R. O. Buckius, Int. J. Mod. Phys. C **9**, 1393 (1998).
[50] A. J. Wagner and L. Qun, Physica A **362**, 105 (2006).
[51] Q. Li and A. J. Wagner, Phys. Rev. E **76**, 036701 (2007).
[52] Q. Li, Ph.D. thesis, North Dakota State University, 2006.
[53] E. B. Perez and M. S. Carvalho, J. Eng. Math. **71**, 97 (2010).
[54] S. Y. Heriot and R. A. L. Jones, Nat. Mater. **4**, 782 (2005).
[55] M. Sasaki, W. J. Suszynski, M. S. Carvalho, and L. F. Francis, J. Coat. Technol. Res., http://link.springer.com/article/10.1007%2Fs11998-012-9444-4.
[56] K. Kim, H. S. Kwak, S. H. Park, and Y. S. Lee, J. Coat. Technol. Res. **8**, 35 (2011).
[57] P. C. Philippi, L. O. E. Dos Santos, L. A. H., Jr., C. E. P. Ortiz, D. N. Siebert, and R. Surmas, Phil. Trans. R. Soc. A **369**, 2292 (2011).
[58] M. Sbragaglia, H. Chen, X. Shan, and S. Succi, Europhys. Lett. **86**, 24005 (2009).
[59] M. Sbragaglia, R. Benzi, L. Biferale, S. Succi, and F. Toschi, Phys. Rev. Lett. **97**, 204503 (2006).
[60] J. Zhang and D. Y. Kwok, Langmuir **20**, 8137 (2004).
[61] J. Zhang and D. Y. Kwok, Langmuir **22**, 4998 (2006).
[62] F. Diotallevi, L. Biferale, S. Chibbaro, G. Pontrelli, F. Toschi, and S. Succi, Eur. Phys. J. B (submitted).
[63] S. Chibbaro, Eur. Phys. J. E **27**, 99 (2008).
[64] L. Biferale, R. Benzi, M. Sbragaglia, S. Succi, and F. Toschi, J. Comput. Aided Mater. Des. **14**, 447 (2007).
[65] A. Mazouchi and G. M. Homsy, Phys. Fluids **13**, 2751 (2001).
[66] M. Sukop and D. Thorne, *Lattice Boltzmann Modeling: An Introduction for Geoscientists and Engineers* (Springer, New York, 2006).
[67] C. Cercignani, Trans. Theory Stat. Phys. **2**, 211 (1972).
[68] H. Chen, S. Chen, and W. H. Matthaeus, Phys. Rev. A **45**, R5339 (1992).
[69] S. Hou, Ph.D. thesis, Kansas State University, 1995.
[70] N. S. Martys and H. Chen, Phys. Rev. E **53**, 743 (1996).
[71] S. Hou, X. Shan, Q. Zou, G. Doolen, and W. Soll, J. Comput. Phys. **138**, 695 (1997).
[72] M. A. Spaid and G. M. Homsy, Phys. Fluids **8**, 460 (1996).